Journal of Hydrology: Regional Studies 64 (2026) 103332

Contents lists available at ScienceDirect

Journal of Hydrology: Regional Studies

journal homepage: www.elsevier.com/locate/ejrh

A multivariate approach to drought monitoring: Improving robustness and accuracy through a new drought index in regions with high climate variability, applied to the drought-prone region of Ethiopia

Abebe Kebede [a], Kirsten Warrach-Sagi [b,*], Thomas Schwitalla [b], Volker Wulfmeyer [b], Tesfaye Abebe [c], Tsegaye Tadesse [d]

[a] Faculty of Meteorology and Hydrology, Arba Minch Water Technology Institute, Arba Minch University, Ethiopia
[b] Institute of Physics and Meteorology, Faculty of Natural Sciences, University of Hohenheim, Germany
[c] College of Agriculture, Hawassa University, Ethiopia
[d] National Drought Mitigation Center, University of Nebraska, Lincoln, United States

ARTICLE INFO

Keywords:
Multivariate drought index
Ecohydrological drought
Drought severity
Monitoring
Decision making
Spatiotemporal analyses

ABSTRACT

Study region: Ethiopia
Study focus: Assessing, monitoring, and quantifying drought characteristics to develop early warning systems is crucial for identifying the spatial extent and severity of droughts at regional and local scales especially in regions of vulnerable societies relying on local agriculture. Observations and reanalysis from 1981 to 2022 are analyzed for spatiotemporal droughts in Ethiopia. While standard drought indices like Standardized Precipitation Index and Standardized Soil Moisture Index are based solely on precipitation or soil moisture, a new drought index based on precipitation, potential evaporation, surface temperature, soil temperature, and soil moisture is developed, making the index more robust to climate and land use changes. This new Multivariate Standardized Drought Index (MvrSDI) is evaluated focusing on the severity and duration of 2015 and 2022 droughts in Ethiopia. Results show that spatiotemporal comparisons of MvrSDI at 3-, 6-, and 12-month time scales detect drought severity and duration in each drought-prone region of Ethiopia. Further,Mann-Kendall statistic test identifiy a drought trend between 1981 and 2022 an increasing drought severity.
New hydrological insight for the region: The MvrSDI effectively assesses and monitors drought impacts on agriculture, proving beneficial for stakeholders focused on environmental sustainability and food security. Its multivariate character makes MvrSDI more robust and therefore a valuable tool for drought monitoring and decision-making in regions with high climate variability and land use changes in drought-prone regions like Ethiopia.

1. Introduction

Drought occurs due to a deficit in the hydrological cycle, leading to severe negative impacts on society, the economy, and the

* Corresponding author.
E-mail address: kirsten.warrach-sagi@uni-hohenheim.de (K. Warrach-Sagi).

https://doi.org/10.1016/j.ejrh.2026.103332
Received 29 September 2025; Received in revised form 5 March 2026; Accepted 6 March 2026
Available online 11 March 2026

environment (Aghakouchak et al., 2014; Wardlow et al., 2008).

Several meteorological, agricultural, and hydrological drought indices have been developed (Bae et al., 2019) and show that drought frequency across the globe has increased over the past decades and is predicted to be more severe in the future (Kikstra et al., 2022). This can cause many detrimental impacts on the environment and economy (Mishra and Singh, 2010; Rulinda et al., 2012). In arid and semi-arid regions of Africa, moderate to severe droughts have been recorded in the 1960, 1970, and 1980s (Dike et al., 2020).

The Horn of Africa is severely and frequently affected by drought due to a deficiency of precipitation (Sawada and Koike, 2016), which directly propagates to deficiency of soil moisture. Due to a variety of meteorological, environmental, and societal factors, Ethiopia has experienced periodic droughts and catastrophic droughts (Gebrehiwot et al., 2011; Bayissa et al., 2015). Famine is brought on by drought, according to long-term drought records (Viste et al., 2013). Over the past nine centuries, Ethiopia has had over 30 major drought occurrences, 13 of which were severe enough to damage the entire country (Gebrehiwot et al., 2011; Bayissa et al., 2015). Ethiopia experienced its first known famine brought on by drought in 1973–1975 (Wagaw et al., 2005). The two droughts with the highest death tolls occurred between 1973–1975 and 1984–1985, while the drought that impacted the largest population was in 2002–2003 (Degefu and Bewket, 2015). The 2002–2003 severe drought in Ethiopia was alleviated by the government providing food aids to alleviate the crisis instead of preparing to mitigate such drought before it occurred. This drought was more severe and widespread than the most extensive one in 1984–1985 (Funk et al., 2015). In 2010–2011, Ethiopia was affected by drought; however, its effect was managed (Gebrehiwot et al., 2011; Bayissa et al., 2015; Degefu and Bewket, 2015).

Various studies on drought analysis, monitoring systems, and prediction have been conducted using either the Palmer Drought Severity Index (PDSI) (Palmer, 1965; Vicente Serrano et al., 2011) or Standardized Precipitation Index (SPI) (Palchaudhuri and Biswas, 2014; Fuentes et al., 2022). Based on timescales, SPI extracts information used for meteorological drought (Adnan et al., 2015), agricultural drought (Kaniewski et al., 2012), and hydrological drought (Tigkas et al., 2017) monitoring.

Before 1970, the probability of a drought occurring was once every ten years. However, since then, droughts have become more frequent (Gebrehiwot et al., 2011). Recently, droughts have been occurring at least every two to three years, varying in severity and duration. Thus, monitoring fluctuations in drought conditions over extended periods is essential for a variety of applications (Heydari et al., 2018; Mahmoudi et al., 2019).

Since the late 2020, following three consecutive poor rainy seasons the pastoral areas of southern and southeast Ethiopia have been affected by drought when compared to historical rainfall seasons (Devi, 2022; FEWS NET, 2021). Drought conditions cause reduction in crop production and vegetation cover, impacting forage and livestock conditions, and this eventually affects food security and livelihoods of communities (Matere et al., 2020). The PDSI relies on soil water availability and temperature, whereas the SPI is derived from a precipitation probabilistic approach. Numerous studies indicate that depending solely on a single drought index may not adequately capture the various aspects of drought onset, duration, and severity (Aghakouchak, 2015). Hao and AghaKouchak (2013) found that while precipitation can quickly signal the onset of drought, soil moisture provides a more accurate depiction of drought persistence.

To develop drought indicators that take multiple variables into account, the nonparametric method can be extended to higher dimensions (Farahmand and AghaKouchak, 2015). In their study, Hao and AghaKouchak (2014) analyzed the bivariate distribution of precipitation and soil moisture, both of which are related to drought. By considering the joint probability of two or more drought-related variables, the empirical probability can be calculated using the multivariate model of the Gringorten plotting position, as introduced by Yue et al. (1999). Scientific techniques for analyzing droughts include probability methods (McKee et al., 1993), Gringorten plotting position (Gringorten, 1963), and the Vegetation Drought Response Index (Wardlow et al., 2008). However, the use of logarithmic algorithms for assessing, monitoring, or forecasting droughts is not common for single or multiple variables. Additionally, there is a lack of non-parametric approaches to multivariable drought analysis that can effectively characterize, monitor, and predict drought conditions in Ethiopia, which would enhance the early warning system.

This research aims to examine the performance of a newly developed multivariate drought index (MvrSDI) in relation to various types of droughts that have occurred in Ethiopia, both at the national and local levels. The MvrSDI is based on five variables derived from in-situ measurements and earth observation data, which assess meteorological and agricultural drought conditions in Ethiopia. It used to create and test a reliable MvrSDI that incorporates key agro-climatic variables in order to accurately assess, monitor, and characterize the spatiotemporal patterns, severity, and trends of droughts in Ethiopia from 1981 to 2022, with the goal of improving early warning systems and promoting agricultural resilience and food security. The findings are expected to help in monitoring drought conditions and developing an early warning system that employs a new approach to enhance agricultural extension services.

2. Data and methods

2.1. The study area: Ethiopia

The study area covers all parts of Ethiopia, which is bordered by Kenya to the south, Somalia to the east and south-east, South Sudan, Sudan to the west, Djibouti to the east, and Eritrea to the north located at 3–15°N and 33–48°E in the Horn of Africa. Based on topographic variation, Ethiopia has three main traditional climatic zones that include *Kolla* (i.e., warm semiarid with altitude less than 1500 m above sea level), *Woina dega* (a cool semi-humid temperate zone with an altitude of 1500–2400 m above sea level), and *Dega* (i.e., a cool and humid zone with an altitude that range from 2400 to 3200 meters above sea level). Areas above 3200 m.a.s.l. are referred as Alpine zones, and not very suitable for crop production due to the very low temperature. The country has a temperate climate in the highlands and a tropical climate in the lowlands, with the main rainy season from mid-June to mid-September (Berhanu et al., 2014). Ethiopia experiences three distinct rainy seasons based on climate: February-May (FMAM, Belg), June-September (JJAS, Kiremt), and

October-January (ONDJ, Bega) south and south eastern parts of Ethiopia (Diro et al., 2011). The primary rainy season is June through August, when many regions of the nation see heavier rainfall than other seasons.

Most of Ethiopia experiences its smallest rainy season in FMAM. During this period, temperatures reach their highest levels, and rainfall varies significantly both spatially and temporally (Teshome and Zhang, 2019). In contrast, the southern and southeastern regions of the country receive increased precipitation during ONDJ. The southwest and northwest regions of Ethiopia experience the highest average annual rainfall, ranging from 1750 to 2250 mm (Teshome and Zhang, 2019).

Ethiopia is prone to frequent and severe droughts as well as floods, both of which significantly contribute to economic losses. Various regions of the country suffer from drought, resulting in food insecurity (FEWS NET, 2021; Tesso, 2019; Bogale and Erena, 2022; Gisila et al., 2015; Abara and Budiastuti, 2020).

2.2. Data source

This study examines meteorological and agricultural droughts using five drought indices. To calculate the drought indices, we used monthly precipitation data from the Climate Hazards Group InfraRed Precipitation with Station data (CHIRPS). The CHIRPS dataset is designed to monitor climate extremes in a historical context, featuring a horizontal resolution of 0.050 × 0.050 ° and temporal coverage from 1981 to the present. This high-resolution gridded data covers latitude from 50°S to 50°N and is employed where station data are unavailable, allowing us to identify both deficit and excess precipitation values (Funk et al., 2015). In addition, land variable datasets are collected from the ERA5-Land of Copernicus climate change data. These global datasets have a spatial resolution of 0.10 × 0.10 ° and provide temporal records from 1950 to the present. We extracted monthly potential evaporation, air temperature at 2 m above the surface, and soil temperature data from the ERA5-Land dataset (Copernicus Climate Change Service (C3S), 2019). The monthly soil moisture data collected from the Earth System Research Laboratory's Physical Sciences Division (ESRL PSD) has a horizontal resolution of 0.50 ° from 1948 to the present day, for the study area (Fan and Van Den Dool, 2004). Various resolutions of gridded data are interpolated to this uniform grid size using the Climate Data Operators (CDO) nearest neighbor remapping method. The Normalized Difference Vegetation Index (NDVI) data downloaded USGS FEWS NET Data Portal provides in support of FEWS NET drought monitoring efforts in the context of East Africa. The USGS FEWS NET Project is part of the early warning focus area at the USGS Earth Resources Observation and Science Center.

2.3. Methodology

The SPI, established by McKee et al. (1993), is commonly used as a univariate measure of drought. Hao and AghaKouchak (2013) suggested the development of a multi-index model using the joint distribution of multiple univariate drought variables. This study introduces the Multivariate MvrSDI, which is based on a logarithmic function and incorporates a formula that used to assimilate five variables: soil moisture, air temperature, soil temperature, precipitation, and potential evaporation. The SPI, SMI, and MvrSDI are compared with observational data to assess historical drought trends and recent occurrences.

In this study, we compared the new approach of drought indices based on logarithmic function with empirical approach of the marginal probability derived using the univariate form of the Gringorten plotting position formula expressed by (Gringorten, 1963) as:

$$p(x_i) = \frac{i - 0.44}{n + 0,12} \tag{1}$$

where i is the rank of the observed values from the smallest and n is the number of the observations. In other words, the SPI and SMI are derived by standardizing the marginal probabilities as described by the Gringorten plotting position formula in Eq. 1.

Instead of fitting a parametric distribution function, the probabilities of observed precipitation and soil moisture are computed empirically. The empirical probabilities are then standardized as SPI=$\varnothing^{-1}(p_p)$ and SMI = $\varnothing^{-1}(p_s)$ where $\varnothing$ is the standard normal distribution (probability density function), and probability of precipitation (p_p) and probability of soil moisture (p_s) denote the empirical probabilities of precipitation and soil moisture, respectively.

standardized drought analysis tools (sdat) and the new approach using logarithmic functions (log), are compared to investigate the new drought approach performance. This tool works based on lag association based on each time scale (see Fig. 6); however, the logarithmic approach has no lag association for each time scale. Based on this evidence during comparison, both drought indices in the context of Ethiopia, the logarithmic approach of drought SPI12log, SMI12log and MvrSDI12log show lags on drought characteristics such as severity, onset, persistence and offset drought in comparison to standardized drought analysis tools. Since Ethiopia is frequently affected by drought, developing and exploring drought is valuable for various sectors. The catastrophic drought hit Ethiopia during the mid-1980s (USAID 1985; Pankhurst, 1990) and that was also captured by both SPI12sdat and SPI12log precipitation deficit (Fig. 6).

The temporal MvrSDI of Addis Ababa, Mekelle, Liben, and Borena were compared with the SPI and SMI. The SPI, MvrSDI, and SMI drought indices were explored for the time scales of 3-,6-, and 12-month during the period of 1981 – 2022. In the following the number behind the index gives the timescales, e.g. SPI6 is the SPI for a 6 months timescale. Different locations are selected to evaluate the performance of MvrSDI using climate data from 1981 to 2022.

The trends in seasonal rainfall maximum and minimum temperatures over the regions of Ethiopia were computed by fitting a linear regression model to each grid cell, and the significant differences in the trends were assessed using the Mann-Kendall test to investigate the four homogeneous climatic regions (Ware et al., 2022). These homogeneous climatic regions have distinct annual cycles, seasonal

rainfall and temperature trends, and annual rainfall anomalies (Ware et al., 2022). The homogeneous climatic regions are used for the spatial drought map.

Since the climatic data are gridded datasets with different spatial resolutions, we interpolated to achieve the desired resolution. The climatic components are at a monthly interval and computed using the five potential variables, including precipitation, potential evaporation, air temperature (2 m), soil temperature layer 1 (0–7 cm depth) and layer 2 (7–28 cm depth), and also soil moisture as an input to develop a multivariate drought index.

The ratio of precipitation to potential evaporation is represented by τ_i; τ_i is physically based on the aggregated evaporative demand of the atmosphere and precipitation. It can be more effectively associated with hydrological and agricultural drought and created to study the effects of climate instability conditions (Altieri and Koohafkan, 2008).

$$\tau_i = \frac{Prec}{PE} \tag{2}$$

where, Prec is Precipitation, and PE is Potential Evaporation.

Surface and soil temperatures play critical roles in understanding climate change and its impacts. Increased surface temperatures can lead to more frequent heatwaves, altered precipitation patterns, and shifts in climate zones (Houghton et al., 2001; Intergovernmental Panel on Climate Change (IPCC), 2021). Soil temperature affects seed germination, root development, and plant growth, impacting crop yields and productivity (Lobell et al., 2011). Changes in air temperature influence soil temperature through heat flux and moisture changes, while soil temperature affects surface temperatures through heat storage and release (Fang et al., 2006). For accurate climate modeling, both air and soil temperature data are essential to predict carbon fluxes, agricultural productivity, and overall climate dynamics (Schlesinger and Andrews, 2000). In heat transport from soil to air, the 2-meter air temperature shows a stronger correlation with skin temperature (the Earth's surface temperature) than with upper soil temperature. This is because the air temperature at 2 m is more directly influenced by the surface conditions, which include the skin temperature, rather than by the temperature of the soil beneath.

Surface temperature is an influential variable of energy and the hydrologic cycle, both at a specific and global magnitude (Kleidon and Renner, 2013).

Due to the lag of transport of heat from the soil skin level to the 2-metre air and to underground layers based on depth cannot respond simultaneously (Jin and Mullens, 2014). The lag in heat transport from the soil skin level to the 2-meter air temperature arises from the thermal properties of soil, which include thermal conductivity and heat capacity. When the soil surface warms, it takes time for this heat to propagate upwards due to the slower thermal response of the soil compared to air. This delay is influenced by factors like soil moisture content, with wetter soils exhibiting a longer lag due to higher heat capacity (Liu et al., 2020). As a result, changes in air temperature at 2 m may not reflect immediate fluctuations in soil temperature, impacting local climate and ecological processes (Benson et al., 2018; Wang et al., 2019).

τ_j is represented by the ratio of air temperature to the average values of the two layers of soil temperatures.

$$\tau_j = \frac{T_{air}}{T_{soil}} \tag{3}$$

$$M_i = \quad -\tau_i. \quad \tau_j.\mathrm{SM} \tag{4}$$

where T_{air} is air temperature at 2 m, T_{soil} is soil temperature depth 28 cm, SM is soil moisture and M_i is the multivariate. These coefficients determine the moisture content required for the soil and atmosphere. If dry weather persists, there is a deficit of moisture on the surface and soil, an indication that the dry period has become a drought (Eq. 4).

Extended periods of warmer surface and soil temperatures increase evaporation, resulting in less surface water and drier soils and vegetation (Dai et al., 2018). If these conditions are followed by insufficient precipitation, the weather will become drier.

Evapotranspiration, vegetation stress, soil moisture, and thermal inertia are all measured using land surface temperature (Karnieli et al., 2010). Water stress due to a moisture deficit can cause significant yield losses, especially for crops in sensitive growth stages (Chai et al., 2016).

The probability function (McKee et al., 1993), the Gringorten plotting position (Gringorten, 1963), and in this research, a new approach of logarithmic function is used to quantify the SPI, SMI, and MvrSDI. The logarithmic function used in modeling, analyzing drought and drought-related issues due to its capturing abilities of exponential growth or decay patterns and efficiently identify relationships by compressing large values, making them useful for analyzing data of varied magnitudes. In comparison to other models, logarithmic function provides a more realistic and scalable approach to assessing the complex and dynamic character of drought periods. It strengthens the methodological basis for predicting and managing drought risk. Based on the new approach of logarithmic function the SPI, SMI, and MvrSDI are calculated.

$$lm_i = \log M_i \tag{5}$$

$$\mathrm{MvrSDI} = \quad \frac{lm_i - \overline{lm_i}}{\delta_i} \tag{6}$$

Where lm_i individual values, $\overline{lm_i}$ is the mean values and δ_i is standardized deviation

A similar logarithmic algorithm is used to investigate the SPI and SMI and identify the drought condition. According to McKee et al.,

(1993), drought starts when the SPI falls below zero and ends when it becomes positive.

According to Kebede et al. (2020), the threshold SPI ≤ -1 was used in this study to identify and analyze all drought occurrences, ranging from moderate to extreme. This value is also implemented for SMI and MvrSDI (Table 1).

2.3.1. Cronbach's alpha test

Cronbach's alpha (CA) test was used to assess the reliability of the indices across the 3-, 6-, and 12-month time scales. The CA test is used to ensure the coherence and accuracy of items in a measurement tool during development and validation. This statistical measure is crucial for evaluating the quality of a scale or test, determining its reliability, and assessing internal consistency SPI, SMI and MvrSDI for various locations.

The CA coefficient formula carries specific significance is expressed as:

$$\alpha = \frac{k}{k-1}\left(1 - \frac{\sum_{i=1}^{k} \delta^2}{\sigma_{total}^2}\right) \tag{7}$$

Where, k represents the number of items on the scale, crucial for assessing the scale's measurements. A higher k indicates a greater number of elements being measured; σ_i^2 describes the variance of each item, gauging the extent to which scores for each item vary. σ_{total}^2 signifies the variation in total scores obtained from all the three drought indices (SPI, SMI, and MvrSDI) on the scale, determining overall variability in drought indices scores by incorporating each component and it illustrates the entire range of variance present in the scale. CA evaluates the vital for evaluating internal consistency. CA interpretation values are depicted in the Table 2.

Values of CA range from 0 to 1, where a higher value indicates greater reliability and the alpha value of 0.7 or above is considered acceptable, indicating that the indices for similar time scales of SPI, SMI, and MvrSDI on a test are correlated and consistent. The data you provided represents different time scales for various stations, which could be evaluated through Cronbach Alpha to assess how consistently the time scale measures specific characteristics in those stations. In the case of the provided dataset for different stations, the values represent some form of measurement across three different time scales (3-, 6-, and 12-month time scales). These time scales of drought indices show slight variations for each station, and calculating the CA across these values would give insight into the internal consistency of the measurements. The time scales show reliability that suggests the fluctuations in the measured values across time are consistent within each station, meaning that changes over time are somewhat predictable and can be interpreted reliably.

2.3.2. The Mann–Kendall trend test

This study investigates the trends in the SPI at a three-month, six-month and twelve-month time scales SPI6, along with the SMI6 and MvrSDI6 drought indices across multiple stations. The analysis of these indices from 1981 to 2022 will determine whether there are increasing or decreasing trends in drought conditions across various geographic locations. To assess these trends, we utilize the normalized test statistic (Z). A positive Z value indicates an increasing trend, while a negative Z value denotes a declining trend (Omondi and Lin, 2023) but for drought the idea negative trend shows increasing drought. The significance of the results is evaluated based on the p-value, with a threshold set at 0.05. A p-value less than or equal to 0.05 suggests a significant trend in the data, while a p-value greater than 0.05 supports the acceptance of the null hypothesis, indicating that no significant trends are present. The Mann-Kendall statistic S for the sequence x is provided by the test (Kendall, 1975; Mann, 1945):

$$S = \sum_{i=1}^{n-1} \sum_{j=i+1}^{n} \mathrm{sgn} x_j - x_i \tag{8}$$

Where x_j and x_i are the annual values for years j and i, j > i, and n is the number of data points, and

$$Sgn\,(xj - xi) = \begin{cases} 1: & if\ xj - xi > 0 \\ 0: & if\ xj - xi = 0 \\ -1: & if\ xj - xi < 0 \end{cases} \tag{9}$$

A positive value of S indicates that the trend is increasing, while a negative value of S indicates that the trend is decreasing.

Table 1
Event classification based on drought indices values.

Indices Values	SPI Classes
Extremely wet	≥ 2.0
Severely wet	1.5–2.0
Moderately wet	1.0–1.5
Mildly wet	0–1.0
Mildly drought	-1.0–0
Moderate drought	-1.5 to −1.0
Severe drought	- 2.0 to −1.5
Extreme drought	≤ -2.0

Table 2
Cronbach's alpha (α)interpretation.

Cronbach's alpha (α)	Internal consistence
$\alpha \geq 0.9$	Excellent
$0.9 > \alpha \geq 0.8$	Good
$0.8 > \alpha \geq 0.7$	Acceptable
$0.7 > \alpha \geq 0.6$	Questionable
$0.6 > \alpha \geq 0.5$	Poor
$0.5 > \alpha$	Unacceptable

The variance of S is s denoted by

$$Var(S) = \frac{1[n(n-1)(2n+5) - \sum_{t}^{g} f_t(f_t-1)(2f_t+5)]}{18} \tag{10}$$

Where t varies over the set of tied rankings and the frequency with which rank t appears is given by f_t. The following test statistic is used by the Mann-Kendall (MK) Test:

$$Z = \begin{cases} \dfrac{S-1}{\sqrt{Var(S)}}, & S > 0 \\ 0, & S = 0 \\ \dfrac{S+1}{\sqrt{Var(S)}}, & S < 0 \end{cases} \tag{11}$$

The presence of a statistically significant trend is evaluated using the Z value. In this study, a 95% confidence level was established, leading to the rejection of the null hypothesis if $|Z| > 1.96$. A higher magnitude of the Z value indicates that the trend is statistically significant. At the significant level of 0.05, the null hypothesis, which posits that there is no trend, is rejected if the absolute value of Z is greater than 1.960. If Z is positive, the data sequence shows an upward trend; conversely, if Z is negative, it shows a downward trend. The MK Z-value > 1.96 shows a significantly increasing trend, and < -1.96 shows a significantly decreasing trend at 5% significance level (Saddique et al., 2020). The null hypothesis is not rejected at the 95% significance level where –1.96 < z < 1.96.

2.3.3. Sen's slope method (β)

Sen's slope is a nonparametric estimate of the slope of a time series to used estimate the degree of a trend that occurs in the time series (Gocic and Trajkovic, 2013). Sen's slope is a robust estimate of the trend magnitude. The slope estimator β is a median of all possible combinations of values for the whole data set. A positive value of β suggests that the trend is up, while a negative value suggests the trend is down (Nalley et al., 2013). During the process of calculating of Sen's slope, all sets of slopes (m_{ij}) are calculated using the Equation below for each pair of y_i and y_j. Then, the Sen Slope (β1) is calculated as the median of all slopes, *mij* using the formula for β1 below.

Each set of slopes (m_{ij}) is computed using

$$m_{ij} = \frac{y_j - y_i}{j - i} \tag{12}$$

Where i = 1, 2, 3… (n − 1) and j = 2, 3… N, while y_j and y_i are data values at time j and i (j > i), respectively.

The median of the n values of m_{ij} is represented by Sen's slope of estimation given by $\beta 1 = m\left(\frac{n+1}{2}\right)$ for n is odd, and $\beta 1 = \frac{1}{2}[m(\frac{n}{2}) + m(\frac{n}{2}+1)]$ for n is even (Nalley et al., 2013).

2.3.4. Pearson's correlation coefficient

The standardized monthly smoothed temporally NDVI was calculated using remote sensing data from Earth Explorer using FEWS Net images for the years 2006 and 2022 for the 12 months. The spatially labeled picture file format was used to collect all of the FEWS NET data. The MvrSDI calculated based on 1, 3, 6, and 12 time scales for the years 2006 and 2022. By standardize monthly smoothed temporally NDVI correlate with MvrSDI across various time scales. The R is calculated as:

$$R = \frac{\sum (x_i - \overline{x})(y_i - \overline{y})}{\sqrt{(x_i - \overline{x})^2}\sqrt{(y_i - \overline{y})^2}} \tag{13}$$

3. Results and discussion

The MvrSDI considers five important agro-climatic variables, that is, precipitation, potential evaporation, air temperature, soil temperature, and soil moisture, reflecting meteorological and agricultural drought conditions; hence, it is a more comprehensive and

robust drought index than SPI and SMI. Unlike SPI and SMI, which are univariate, MvrSDI integrates multiple drought indicators with an assimilation algorithm and a logarithmic transformation that enables the detection of complex drought characteristics, improvement in spatiotemporal assessment, and manifestation of increasing drought trends. It has a capacity to detect complex drought conditions of delayed rainfall, early season heat waves, rapid evaporation losses and soil moisture depletion and land cover changes. The multimodality of MvrSDI will make the index excellent for regions characterized by high climate variability and land-use change, such as Ethiopia.(Fig. 1)

3.1. The spatial distribution of drought in 2015

During JJAS (Kiremt season) 2015 low rainfall due to strong El Niño suppressed precipitation across Ethiopia (Wolde-Georgis et al., 2022). This caused major crop failure and pasture loss in northeastern and central highlands (FAO, 2016). According to Kasie et al., (2020) the multivariate drought monitoring tools captured both deficit of rainfall and heat driven moisture loss.

For the seasonal time scale for June to August the SPI3, SMI3, and MvrSDI3 of drought 2015 are depicted in Fig. 2. The SPI3 shows large coverage, severe to extreme in July and August over Ethiopia's southern and southeastern regions. The deficit of soil moisture in the east and central regions of the country is also investigated. The magnitude of the deficit is higher in the southern parts of the country for the three consecutive months. However, the MvrSDI3 shows a similar spatial distribution of the drought pattern except for its severity compared to SPI3 (Fig. 2). Extreme severe drought recorded by MvrSDI3 in July large area coverage in southern and southeastern parts. The northeastern parts of drought conditions show a decrease from June to August by each drought index.

During the 12-month time scale, the northern and central regions of Ethiopia experienced dry conditions from June to August 2015 (Fig. 3). The strong El Niño significantly impacted these areas over two consecutive rainy seasons, both short and long term (Philip et al., 2018). This is regularly the case, e.g. in the year 2015 the drought episodes affected most regions of Ethiopia (Kourouma et al., 2022). According to this study, on a 12-month timescale in 2015 the indices recorded the most extreme drought episodes in the country.

All drought indices indicate an extreme level of severe drought during June over central north and east of the country. However, the soil moisture index decreased over the following two months, July and August. The two drought indices, SPI12 and MvrSDI12, exhibit similar monthly drought patterns. However, the spatial expansion of drought is captured by MvrSDI12. This analysis highlights the drought-prone regions, mainly due to the influence of the strong El Niño phase.

3.2. The spatial distribution of drought in 2022

For the seasonal time scale, we used the SPI3, SMI3, and MvrSDI3 indices to assess drought conditions in Ethiopia for March, April, and May 2022. Fig. 4 shows that SPI3 indicates a widespread moderate drought in western Ethiopia in March, while SMI3 and MvrSDI3 report only partial moderate conditions in that area. For March-May 2022 season, both SMI3 and MvrSDI3 highlight severe and extreme drought in parts of southwestern, northeastern, and the central Rift Valley regions. A soil moisture deficit was noted in these areas during March and April 2022 affects the agriculture and water management system. Notably, the northeastern region experienced an extreme drought event. Overall, the most severe drought conditions were recorded by MvrSDI3 in March 2022 compared to other months.

For the 12-month timescale, wet conditions over the northern and western parts were identified by all the drought indices. For the 12-month time scale, the SPI12, SMI12 and MvSDI12 depicted in Fig. 5 showed exceptional drought conditions in southern and southeastern Ethiopia; whereas the western and northern parts of the country showed no drought. The soil moisture feedback to

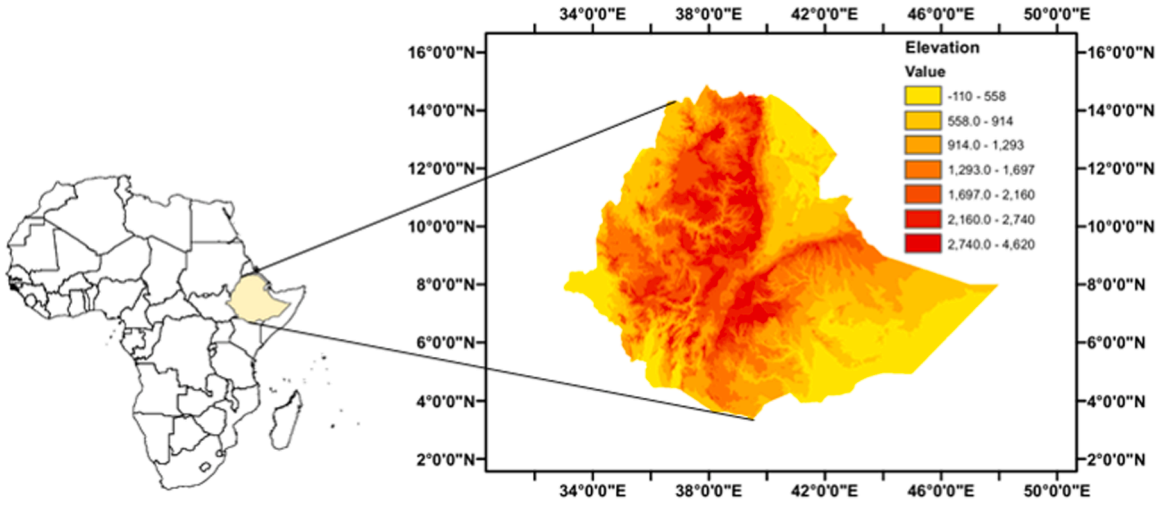

Fig. 1. Location and elevation map pf Ethiopia.

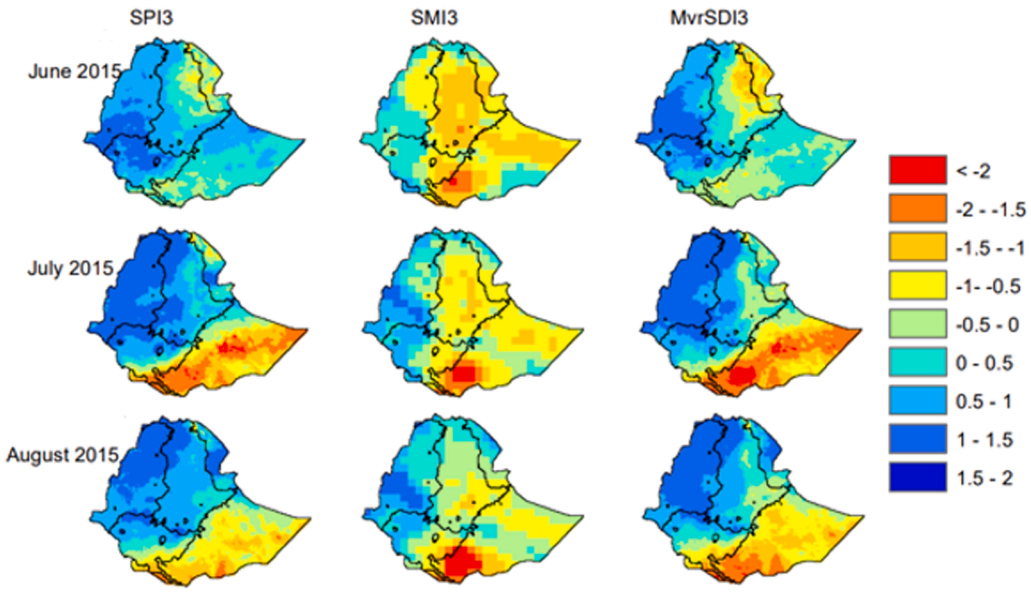

Fig. 2. The three-month time-scale maps of the SPI3, SMI3, and MvrSDI3 for a) June 2015, b) July 2015, and c) August 2015.

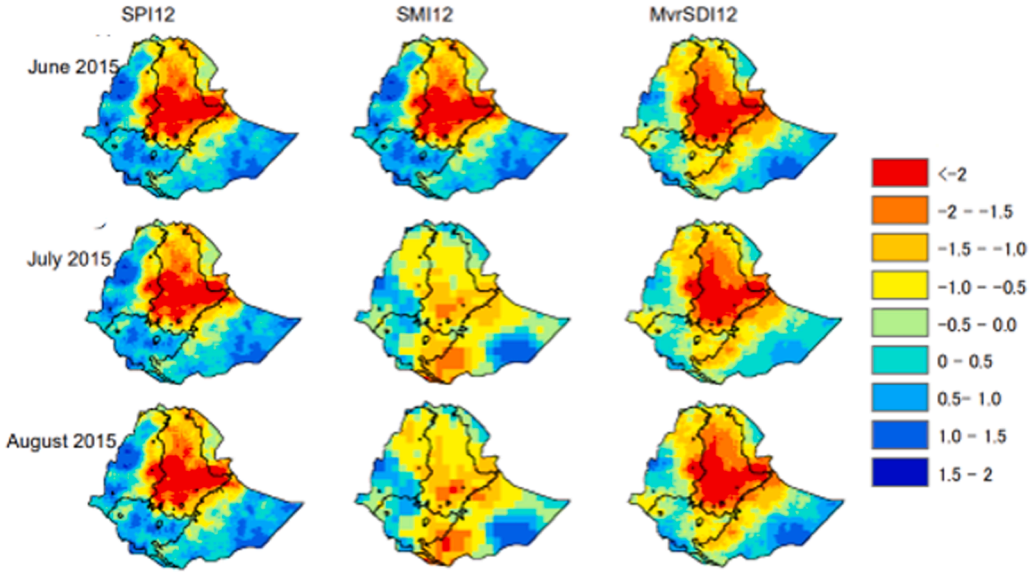

Fig. 3. The SPI12, SMI12 and MvrSDI12 for: a) June 2015, b) July 2015, and c) August 2015.

precipitation indicates the genesis of MvSDI12 with the assimilation of other variables. The SPI12, SMI12, and MvrSDI12 identified severe to exceptional drought conditions in southern and southeastern Ethiopia.(Fig. 6)

Severe to extreme drought conditions were identified in most regions of the southern and southeastern parts of Ethiopia. A large coverage of severe to extreme drought across the drought-prone areas was identified in March as compared to April and May.

Generally, the severity and spatial extent of the drought conditions were captured using 3- and 12-month time scales of precipitation, soil moisture, and combined variables to identify drought conditions in Ethiopia. The MvrSDI3 and 12 time scales have both the characteristics of SPI and SMI of 3 and 12-month time scales. It plays a vital role to determine the transition period of drought propagation. The results showed that these drought indices help in identifying drought conditions and play a vital role in managing drought-prone regions by monitoring different economic sectors.

The drought area coverage based on the values in Table 3 for SPI, SMI, MvrSDI of time scales 3 and 12-month for the months from June to August 2015 and March to May 2022**.** In June 2015 approximately shown normal conditions by SPI3 but SMI3 and MvrSDI3 indicate moderate localized drought and in July 2015 sharp increase in all indices which indicate large-area drought coverage.

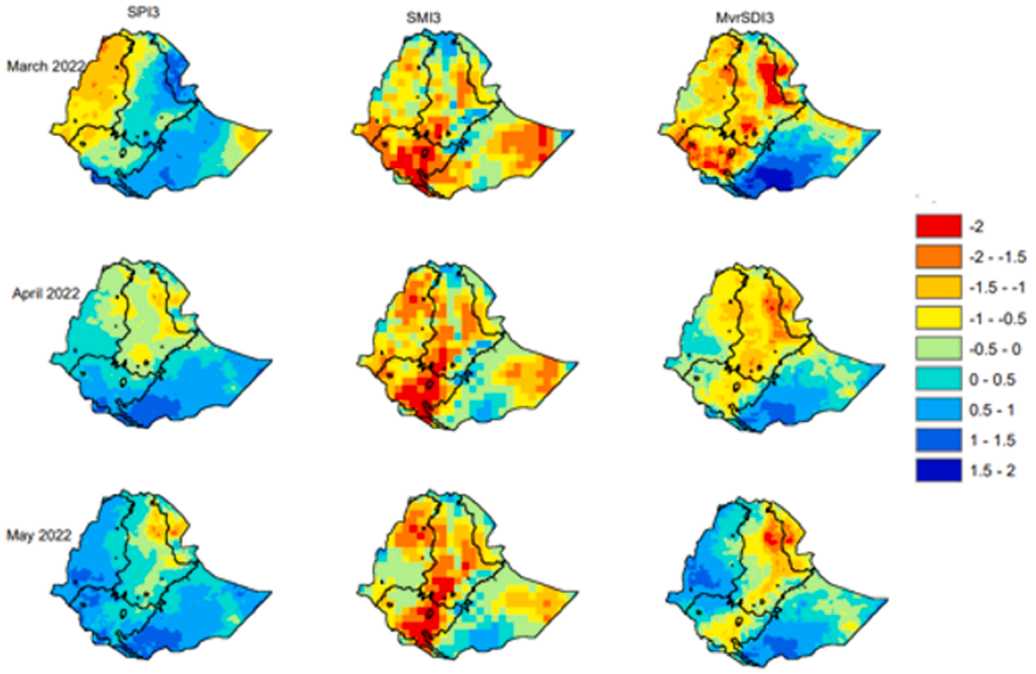

Fig. 4. The SPI3, SMI3, and MvrSDI3 for: a) March 2022, b) April 2022, and c) May 2022.

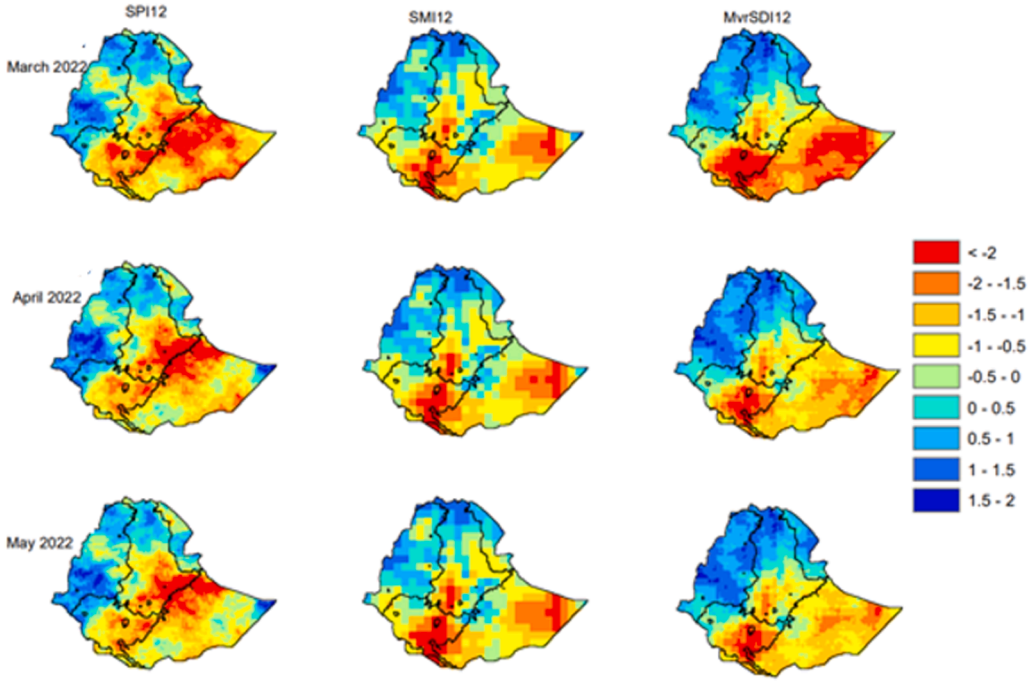

Fig. 5. The SPI12, SMI12, and MvrSDI12 for a) March 2022, b) April 2022, and c) May 2022.

However, in August 2015 lower than July drought persists but coverage area decreased. In 2022 for the three-time scale of SPI suggests near-normal rainfall conditions but SMI3 and MvrSDI3 are high, especially soil moisture in March to April show severe soil moisture deficit, extensive area affected, even if rainfall was not extremely low might be high temperatures, evapotranspiration, or long-term dryness. This shows agricultural drought due to soil moisture deficits.

The long term drought covered large portion of the region by SPI12 and MvrSDI12 in 2015 and in March 2022 shows the highest

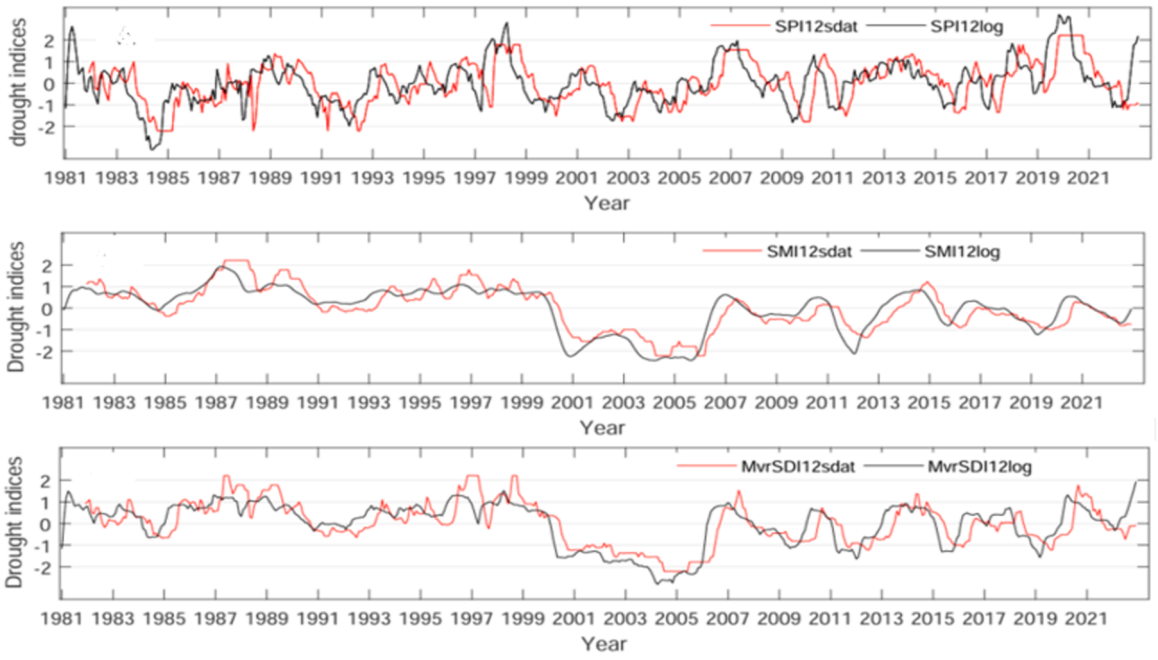

Fig. 6. Comparison of drought indices SDAT and Log for Univariates and Multivariate from 1981 to 2022 over Ethiopia.

Table 3
Percentage areas under drought in the years 2015 and 2022.

	2015			2022		
	June	July	August	March	April	May
SPI3	0.03	9.4	4	0.46	0.44	0.83
SMI3	12.7	5	4.3	25	24.6	18.95
MvrSDI3	1.5	10	7	13	6.5	3.7
SPI12	13.86	13.7	13.5	17.3	13.7	12.08
SMI12	6.4	9.1	10.3	10.9	11.6	12
MvrSDI12	16	16.3	16.4	16.7	14	12

long-term drought values recorded by SPI12 and MvrSDI12 showed extensive and severe long-term drought coverage and decline through May the spatial extent of drought.

3.3. Temporal drought distribution over Ethiopia

The most devastating droughts in Ethiopian history occurred from 1972 to 1974 (Marcus, 1994). The early 2000s drought was influenced by El Niño events and resulted in severe food shortages affecting millions of people (World Food Programme (WFP), 2001; E. K. S., 2002). Such extreme drought events were also shown by SMI12 and MvrSDI12, and extended soil moisture deficit was also investigated, but in the years 2000–2001, severe drought conditions were shown by each approach. In 2009, extreme drought conditions are revealed by SPI12 approaches; however, moderate drought conditions are identified by MvrSDI12log. The 2015–2016 Drought was particularly severe due to the El Niño weather pattern, impacting agricultural production and leading to a humanitarian crisis (FAO, 2016). Such drought severity might be captured by other time scales, the drought situation based on season; however, the dryness is captured each drought approaches.

We evaluated for the time scales 3, and 12. For example, the 12-month timescale was presented for both sdat and the logarithmic function of drought indices. Both types of drought indicators are compared by applying univariate variables (precipitation and soil moisture) and a multivariable approach. As a reference, the standardized drought analysis tool is used to evaluate drought in Ethiopia.

3.4. Temporal drought distribution at different locations in Ethiopia

From the severe to extreme drought episodes identified by SPEI-4 month, in the historical periods of 1983, 1984–1985, 1997, 1998, 1999, 2000, 2003–2004, 2008, 2009, 2015, and 2016 rainy seasons (Kourouma et al., 2022). The 1984 and 2015 were the most severe droughts, mainly affecting the northeastern, northwestern, eastern, and southeastern regions of Ethiopia (Kourouma et al., 2022).

Drought began at the end of 2020 and continues up to 2022 due to a below-average rainy season in a row in the southeastern and southern parts (FEWS NET, 2021). These areas usually receive March-June and October-December rains (Anderson et al., 2023).

This investigation considers different climatic locations are considered to evaluate the performance of MvrSDI for the time scales of 3, 6, and 12 months. Temperature increases are contributing to climate extremes in Addis Ababa and are a result of climate change (Alemu et al., 2021). For Bole Station, severe drought conditions were recorded in 2013; however, drought conditions were noted in 1991, 1996, 2002, and 2011 (Alemu et al., 2021).

Fig. 7 shows the Addis Ababa location of the temporal drought MvrSDI compared with SPI and SMI indices for 3-, 6-, and 12-month time scales. The 3-month frequency of each drought index is higher than a 6- or 12-month time scale. The results for the three and six-month scales show that the frequency of drought severity SPI and MvrSDI are higher than the soil moisture index (SMI) from 1982 to 2006. Beginning from 2007 to 2016, the frequency of drought severity indicated that SMI was higher than SPI and MvrSDI. Such a drought pattern is not seen on the time scale 12-month except by SPI12. For SPI12, drought indices dominated most years over MvrSDI and SMI; however, the drought severity was seen to vary with gradual frequency by SPI, MvrSDI, and SMI in the Addis Ababa location. The drought pattern indicates the moderate to extreme drought phenomenon is captured by each index. The drought onset and offset of MvrSDI3 and MvrSDI6 show similar characteristics to SPI3 and SPI6; however, MvrSDI12 shows closer characteristics to the duration and offset of drought with SMI12 (Fig. 7). It can capture drought conditions for short and long durations of drought.

Mekele is located in northern Ethiopia, which is frequently affected by drought (Menna et al., 2022). An extreme drought that had a significant impact was documented in 1984 in the meteorological data history of the Mekelle Station (Weldesenbet, 2019).

Drought frequency and severity were assessed by SPI, MvrSDI, and SMI indices of the 3-, 6-, and 12-month time scales (Fig. 8). The temporal analysis of drought frequency shows an increase over SPI3, MvrSDI3, and SMI3 over the 6- and 12-month time scales. Drought frequency and severity across 1984–2007 indicated highs over SPI3 and MvrSDI3, SPI6, and MvrSDI6 in the Mekelle location. The MvrSDI 3-, 6- and 12-month time scales show drought severity magnitude next to SPI 3-, 6-, and 12-month time scales for most years. Drought frequency in long time scales of SPI12, MvrSDI12, and SMI12 indices showed less frequency and high duration between 1981 and 2022. The MvrSDI shows characteristics of capturing severe drought and longer duration captured by SPI or SMI.

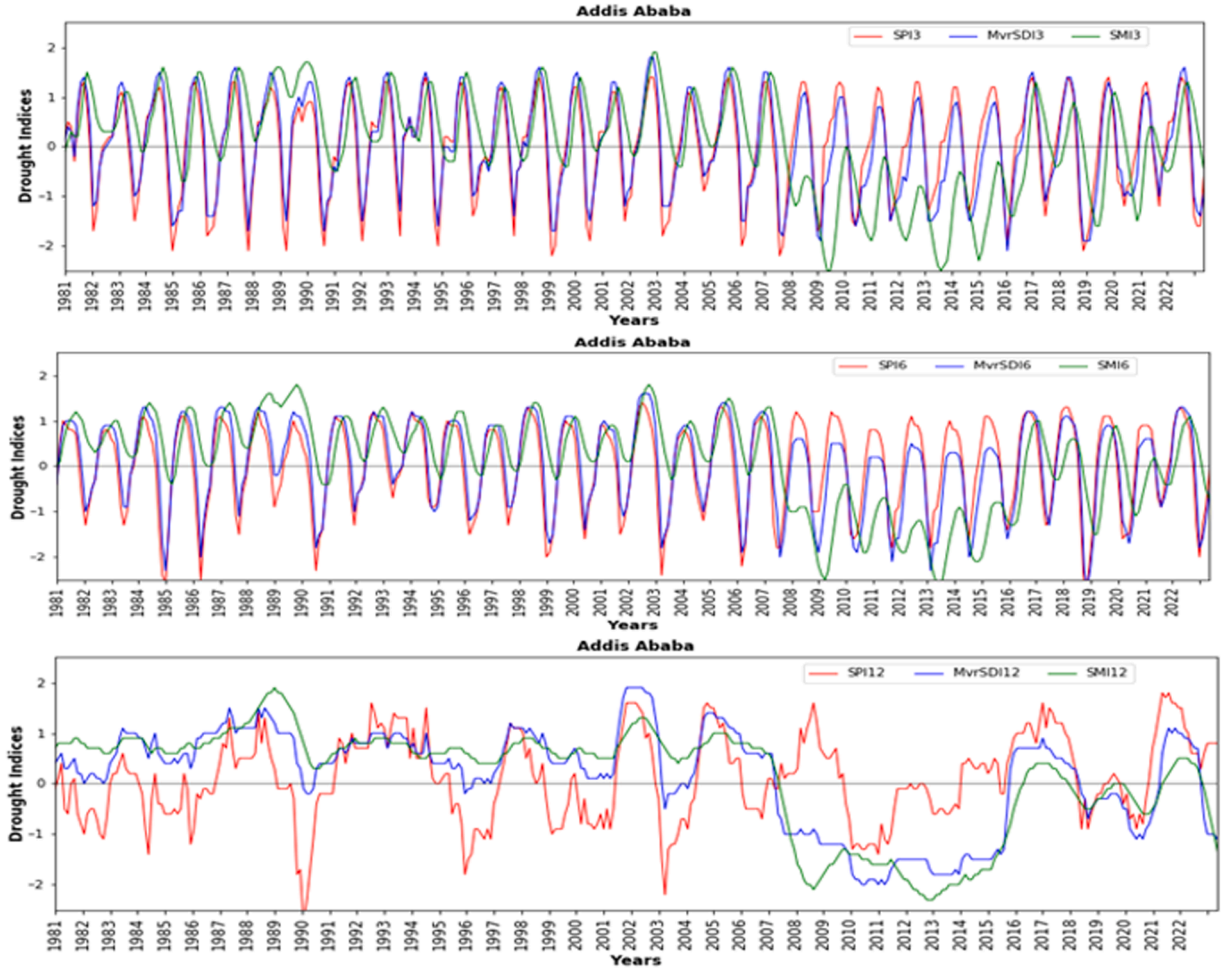

Fig. 7. Temporal drought analysis of SPI, MvrSDI, and SMI indices over 3, 6, and 12 months at Addis Ababa.

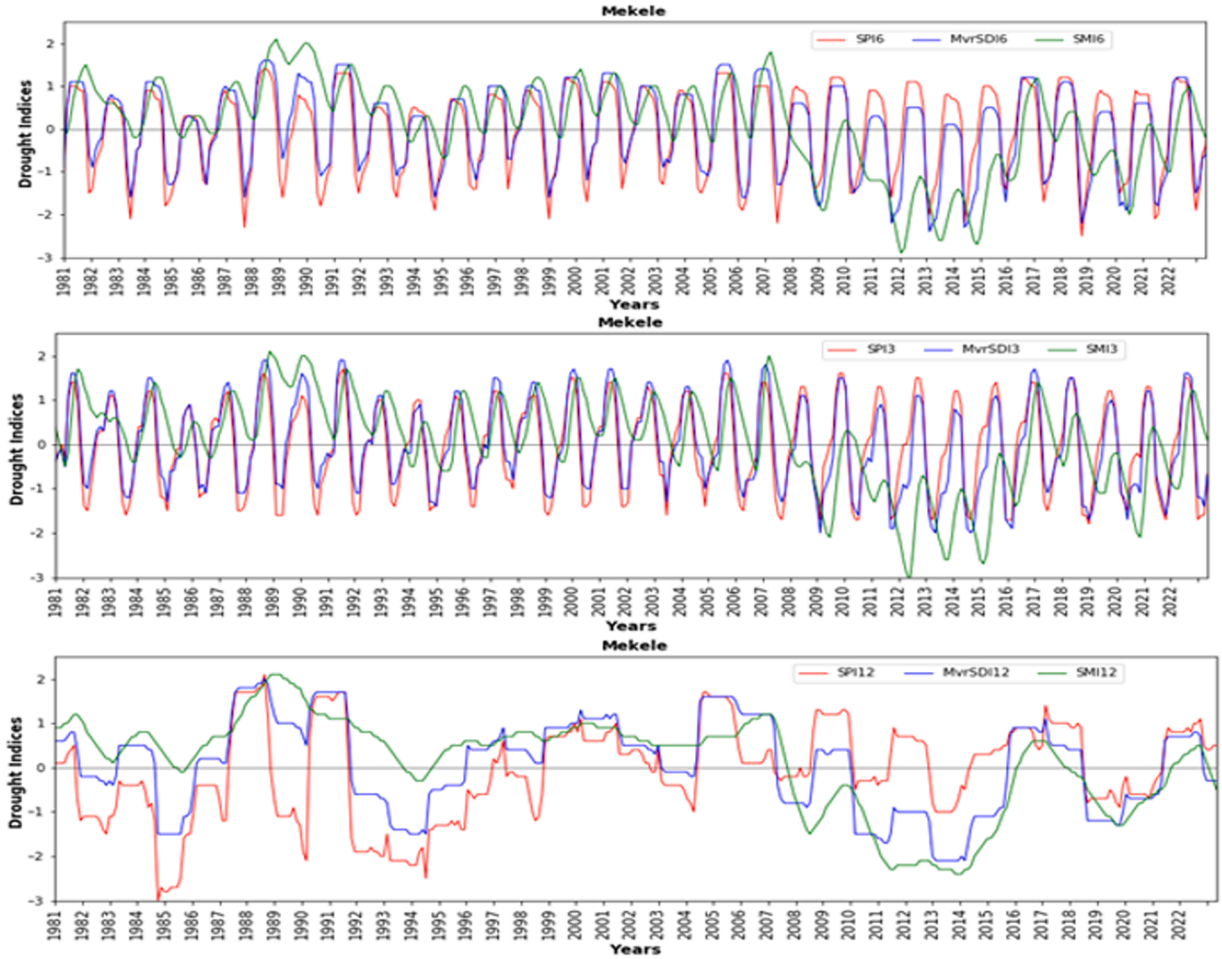

Fig. 8. Temporal drought analysis of SPI, MvrSDI, and SMI indices over 3, 6, and 12 months at Mekele.

Fig. 9 shows the severe/extreme drought conditions captured by the new drought index, also identified by the 3-, 6-, and 12-month SPI, SMI, and MvrSDI. For the 3-month time scale, drought fluctuation was observed compared to 6-and 12-month time scales. Extremely severe drought conditions are identified by the 6-and 12-month compared to 3-month time scales to each drought index. The MvrSDI has the capacity to identify drought magnitude captured by SPI and SMI. A drought begins (onset) due to the rainfall deficit shown by SPI and MvrSDI, persistence and offset of the drought are investigated with lag association to SMI, which is important for an indication phase of the transition period. The 2021 and 2022 severe droughts with long duration were investigated by each drought indices; however, the severity of MvrSDI is the highest.

The drought severely affected the Borana zone for consecutive rainy (Mengistu, 2016). Severe droughts occurred in the wet seasons of 1992, 1999, 2000, 2011, 2019, 2020, and 2021, while extreme droughts were recorded in 1990, 2010, and 2020. The first rainy season of 2011 was the driest year on record. Such a result agrees with Bayissa et al. (2017). The Borena zone is one of the zones frequently affected by drought and needs more attention. Fig. 10 shows the temporal drought condition for the time scales of 6 and 12 months. The severity of the drought is demonstrated by the three drought metrics (SPI, SMI, and MvrSDI) with the highest frequency. This zone is part of the southern regions of Ethiopia, more similar characteristics to the drought conditions to the southern and southeastern parts of Ethiopia. In 1984, 1985, 2000, 2001, 2011, 2017, 2019, 2021, and 2022 severe to extreme severe drought conditions are investigated by SPI, SMI, and MvrSDI of the two consecutive (6 and 12) months of time scales.

3.5. Cronbach alpha test of drought indices

The inter-time scales correlations between SPI, SMI, and MvrSDI at each station is important to identify the consistence. The CA test is largely applied for the purpose of determining internal consistency, which has been commonly applied in this study to determine the reliability/consistency of a set of time scales of drought indices. It is also worth mentioning that the variation in these values across stations, for instance, from 0.65 in Godemet to 0.79 in Debremarkos, may indicate that CA could vary depending on specific characteristics of each station under study and how they are being affected by time scales drought indices.

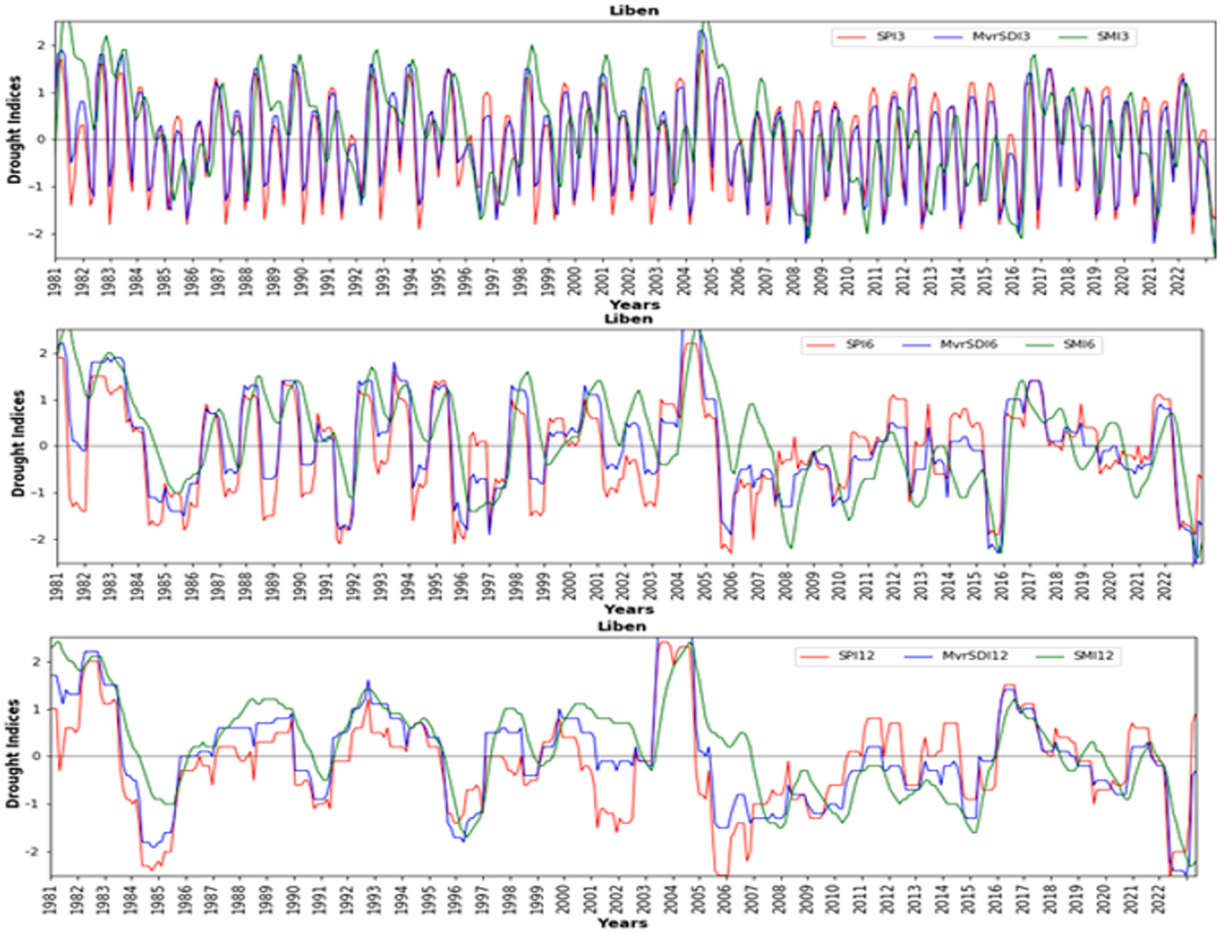

Fig. 9. SPI, SMI and MvrSDI for different time steps: one, three, six and twelve months over Liben Zone.

Except a few time scales of stations, the result alpha is alpha falls below 0.7, it would imply that the drought time scales are less consistent in measuring the same underlying concept and above 0.7, which indicate that there is a good level of internal consistency among the drought indices, suggesting that the values across the different time scales reflect a consistent pattern for that particular station.

Fig. 11 of Godemet ranges between minimum value 0.65 for 3-month time scales and maximum values of 0.90 at 6- and 12-month time scales; this has to lead to lower CA tests, which are indicative of less consistency among time scales. In contrast, Debremarkos is less variable in its values with a range of 0.75–0.80, likely to result in higher CA that are suggestive of strong internal consistency.

3.6. The Mann-Kendall statistical tests and Sen's slope

The MK test results for SPI, SMI, and MvrSDI over 3-month intervals are shown in Table 4. Increasing trends in SPI3 are observed at several stations, meaning there was a rise in precipitation availability over time. The results indicate an increasing trend in SPI3 at the following stations: Arba Minch (Z = 2.8585), Borena (Z = 0.3344), Debremarkos (Z = 0.6845), Gode met (Z = 2.8849), Gonder (Z = 0.9284), Hawassa (Z = 0.8803), Jimma (Z = 1.3354), and Mekelle (Z = 1.1237). A decreasing trend was observed at Addis Ababa (Z = -0.1550) and Bale Robe (Z = -0.3893). Overall, the trends were not statistically significant at the 95% confidence level, except for the stations in Arba Minch and Godemet, where the trends were significantly increasing, meaning these increases in precipitation were likely real in Arba Minch and Godemet stations.

The MK test and Sen's slope estimator were employed to detect trends of SMI values at a 3-month time scale in the study area. In all stations except Godemet station, statistically significant trends were determined for the SMI3-month time scale (Table 4). The results of the SMI 3-month time scale analysis revealed a significant declining trend in nine of the ten stations studied, including Addis Ababa, Arba Minch, Bale Robe, Borena, Debremarkos, Gonder, Hawassa, Jimma, and Mekelle, with Z-values of −8.7062, −9.4698, −4.0440, −10.6230, −4.0758, −3.4436, −7.2173, −4.3427, and −8.8545, respectively (Table 3). This indicates an increasing tendency for drought in these stations. On the other hand, a statistically insignificant upward trend was observed in the SMI3 of station Godemet with a z-score of 1.0021.

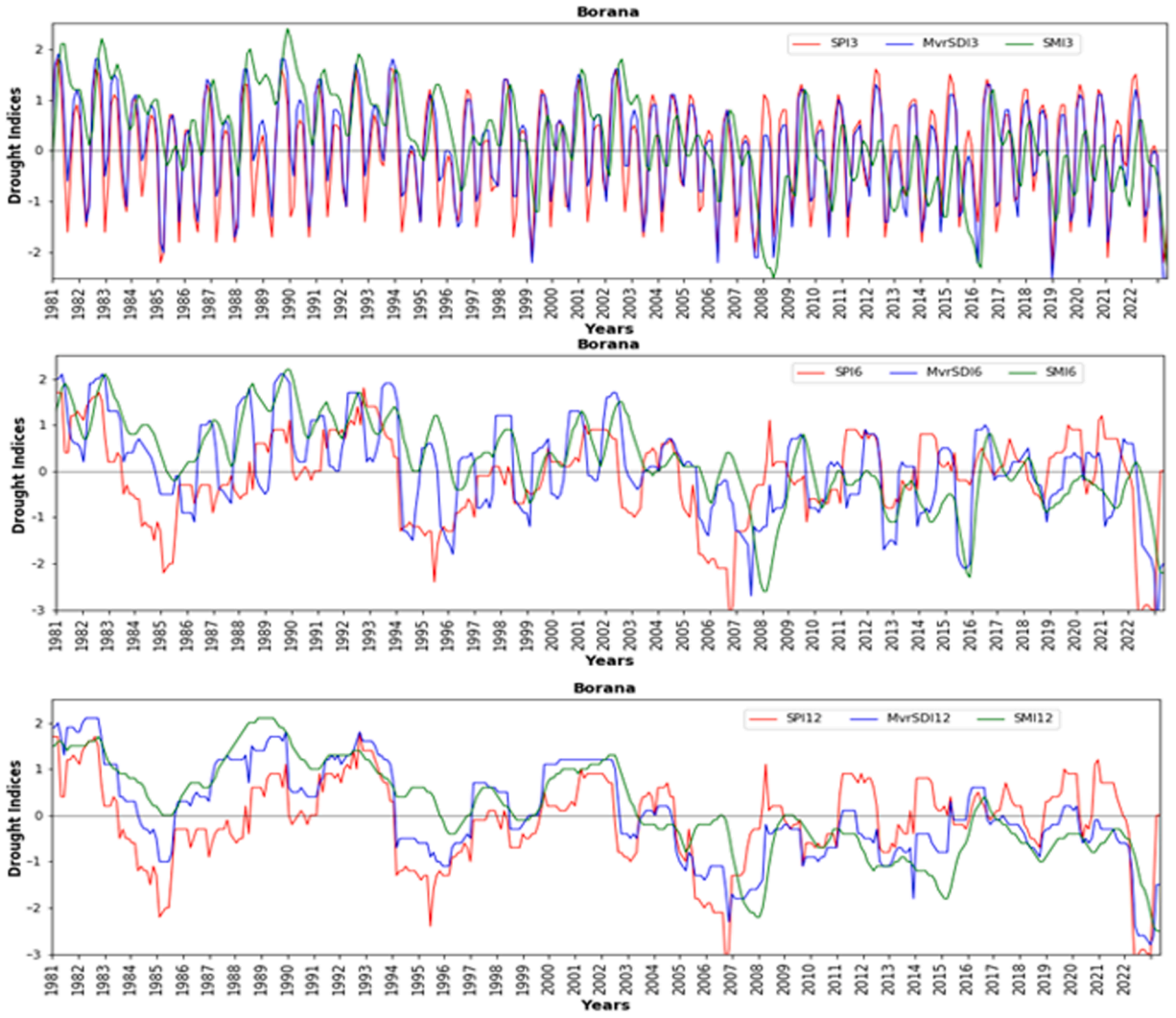

Fig. 10. SPI, SMI, and MvrSDI for different time steps: one, three, six, and twelve months over Borena Zone.

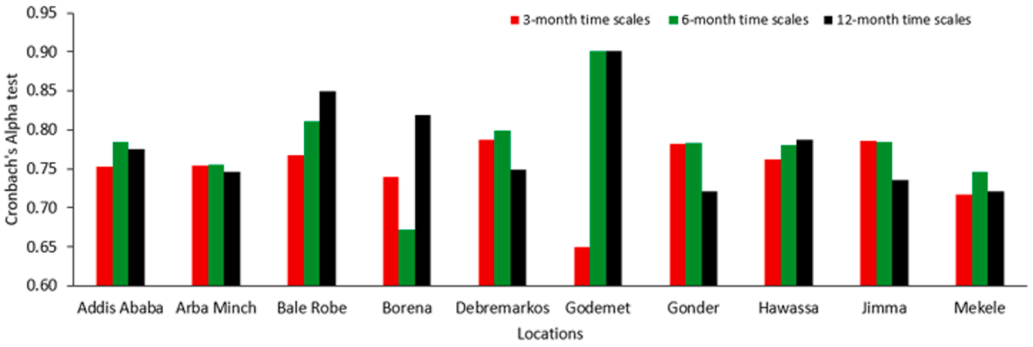

Fig. 11. SPI, SMI and MvrSDI that were used for different time steps: one, three, six and twelve months at different locations Cronbach Alpha test.

Table 3 also presents the results for the MvrSDI3 time scale. Negative Z-values indicate a declining trend in moisture availability, suggesting an increasing frequency and intensity of drought episodes. Addis Ababa, Arba Minch, Bale Robe, Borena, and Hawassa stations exhibited a significant decreasing trend across all MvrSDI3 time scales with Z-values of −2.6848, −2.9355, −2.8210, −3.0531, and −2.4292, respectively; these values indicate a persistent decline in moisture availability over time. The corresponding Kendall's

Table 4
Mann-Kendall statistical tests and Sen's slope for SPI3, SMI3, and MvrSDI3.

Stations	SPI3				SMI3				MvrSDI3			
	z	Kendall's Tau	p-value	Sen's Slope	z	Kendall's Tau	p-value	Sen's Slope	z	Kendall's Tau	p-value	Sen's Slope
Addis Ababa	-0.1550	-0.0046	0.8769	0.0000	-8.7062	-0.2590	0.0000	-0.0026	-2.6848	-0.0799	0.0073	-0.0008
Arba Minch	2.8585	0.0851	0.0043	0.0008	-9.4698	-0.2820	0.0000	-0.0028	-2.9355	-0.0874	0.0033	-0.0009
Bale Robe	-0.3893	-0.0116	0.6970	-0.0001	-4.0440	-0.1210	0.0001	-0.0011	-2.8210	-0.0840	0.0048	-0.0008
Borena	0.3344	0.0100	0.7380	0.0001	-10.6230	-0.3170	0.0000	-0.0032	-3.0531	-0.0911	0.0023	-0.0009
Debremarkos	0.6845	0.0204	0.4937	0.0002	-4.0758	-0.1210	0.0000	-0.0012	-0.6296	-0.0187	0.5290	-0.0002
Gode met	2.8849	0.0861	0.0039	0.0010	1.0021	0.0299	0.3163	0.0003	0.8545	0.0254	0.3929	0.0002
Gonder	0.9284	0.0276	0.3532	0.0002	-3.4436	-0.1030	0.0006	-0.0011	-0.2632	-0.0078	0.7924	-0.0001
Hawassa	0.8803	0.0262	0.3787	0.0002	-7.2173	-0.2150	0.0000	-0.0022	-2.4292	-0.0723	0.0151	-0.0007
Jimma	1.3354	0.0398	0.1817	0.0003	-4.3427	-0.1290	0.0000	-0.0011	-0.7505	-0.0223	0.4530	-0.0002
Mekelle	1.1237	0.0335	0.2611	0.0003	-8.8545	-0.2640	0.0000	-0.0027	-1.8322	-0.0545	0.0669	-0.0006

Tau values are also negative, reinforcing the downward trend. Moreover, the p-values for these stations are below 0.05, confirming that these trends are statistically significant and unlikely to be due to random chance. In contrast, stations such as Debremarkos, Gonder, Jimma, and Mekelle show weak or statistically insignificant trends in their MvrSDI3 values. Their relatively small negative Z-values (with higher p-values) suggest that while some of these stations may experience periodic dryness, the trend is not strong enough to be considered significant. On the other hand, Godemet is the only station with a positive Z-value of 0.8545, indicating a slight increase in moisture availability rather than a drying trend. However, its p-value of 0.3929 suggests that this trend is not statistically significant.

3.7. Response of standardized temporally smoothed monthly NDVI to MvrSDI

The impact of drought on vegetation is severe (Jiang et al., 2022; Ge et al., 2021) and results water scarcity in the soil, the process of plant photosynthesis decelerates (Wang et al., 2019), leading to desiccation and shedding of foliage including stunted or halted growth. In ecosystems, drought can also lead to a reduction in vegetation (Yuan et al., 2020), soil structure damage, and ultimately land desertification. Drought has a severe impact on vegetation, with significant consequences for both ecosystems and human society (Li et al., 2024).

The relationship between MvrSDI and standardized NDVI anomaly mainly reflects the impact of climate variables, soil conditions on plant growth and health. Water scarcity can lead to plant stress, which in turn affects its photosynthesis and growth, resulting in a decrease in NDVI. The availability of water in different growing seasons can have a significant impact on the plant's photosynthesis and growth rate. For example, in the dry season, NDVI may decrease due to insufficient water; in the wet season, when MvrSDI is high, NDVI will increase accordingly. The hydrologic cycle when soil moisture is sufficient, plant roots can obtain more water and nutrients, which can promote a higher NDVI. Different ecosystems respond differently to water changes (Liu et al., 2024), such as forests, grasslands, and farmlands, and changes in MvrSDI may also affect the availability of water in these ecosystems and subsequently affect NDVI.

The impact of temperature on vegetation growth is profound but the water cycle at normal condition MvrSDI-1 to MvrSDI-12 time scales exhibits heightened sensitivity towards vegetation growth as indicated in Table 5. Furthermore, the expansion of a positive correlation between drought and NDVI occurs for the 2006 and 2022. For 2006 MvrSDI shows decreasing as the function of time scale increases over Ethiopia; however, this condition not observed in the year 2022. This shows that the MvrSDI exerts maximal influence on NDVI. According to the dynamic transmission laws of positive correlation coefficient at various levels of time scales, it is evident that strong and moderate positive correlations exhibit distinct transmission patterns. The most significant positive impact on NDVI comes from MvrSDI-3 of 2006 and MvrSDI-6 of 2022.

The relationship between MvrSDI at the time scales of 1,3,6 and 12 months standardized anomaly of of NDVI for the year 2006 shows that vegetation conditions were most strongly influenced by short-term moisture variability. The 1st and 2nd (1-month and 3-month) time scales exhibit very strong positive correlations of 0.91 and 0.93, showing that that vegetation responded rapidly to immediate changes in drought conditions. As the time scales increases the strength of the correlation declines which implies that vegetation in 2006 was more sensitive to short-term rainfall and moisture variations than to prolonged, long-term drought conditions.

The association values between the MvrSDI at the 1-, 3-, 6-, and 12-month time scales and the standardised NDVI anomaly for the year 2022 show consistently strong positive and showed the strongest response to medium-term drought conditions, as reflected in the highest correlation at the 6-month time scale (0.87), suggesting that cumulative moisture deficits over several months had the greatest influence on vegetation growth or health. The strong positive associations, highlighting that vegetation remained sensitive to both short-term and long-term drought variations, though slightly less than the medium-term effects. In this year the vegetation condition was closely linked to drought severity across all time scales; however, the 6-month drought duration is the most pronounced response.

4. Conclusions

The severity and spatio-temporal drought were investigated MvrSDI over the homogenous climatic regions. MvrSDI used for the planning, management, understanding the characteristics of drought. For the temporal time scales of the 6- and 12-month time scales, MvrSDI has the ability to determine the drought onset closer or similar to SPI, persistence, and offset of drought results close to SMI results which shows both combined information of drought.

In 2015, the extreme severe drought was investigated in the central and northern parts of Ethiopia by SPI and MvrSDI 12-month time scales from June to August. In this season, the spatial drought 12-month time scale shows a higher magnitude of drought. Severe to extremely severe drought occurred in southwestern, southeastern. and partly eastern Ethiopia from March to May months in the year 2022. The change deficit of soil moisture is slow compared to SPI and MvrSDI, which advances the characteristics of the

Table 5
The correlation between MvrSDI and standardized monthly smoothed NDVI.

Year	Index	NDVI	Year	index	NDVI
2006	MvrSDI1	0.91	2022	MvrSDI1	0.79
	MvrSDI3	0.93		MvrSDI3	0.80
	MvrSDI6	0.74		MvrSDI6	0.87
	MvrSDI12	0.59		MvrSDI12	0.79

multivariable drought condition of MvrSDI. Such a deficit leads to extreme and severe drought occurrences in parts of the southern and central rift valley systems. SMI6 and MvrSDI6 showed the increased trend of drought for each time scale over the selected synoptic stations.

While SPI and SMI are shown for comparison, MvrSDI emphasizes the regions and seasons of drought more clearly because it integrates multiple drought drivers-precipitation, soil moisture, air and soil temperature, and evaporative demand that capture not only rainfall deficits but also heat or energy-driven drying. This allows it to identify agricultural drought in hot lowlands, early-season stress, and locations where soil moisture alone may not indicate drought. By accounting for temperature and evaporation effects, MvrSDI is more sensitive to regions and periods when crop and pasture stress occurs, making it a more physically robust tool for monitoring drought impacts.

The strong positive associations of standardized NDVI monthly anomaly with MvrSDI shows that vegetation remained sensitive to both short-term and long-term drought variations, though slightly less than the medium-term effects.

Thus, spatiotemporal drought analysis using the new approach MvrSDI for each time scale has the ability to capture the drought occurrence probabilities and drought propagation period over the complex orography of Ethiopia used to enhances drought monitoring and early warning systems.

CRediT authorship contribution statement

Abebe Kebede: Writing – review & editing, Writing – original draft, Visualization, Validation, Software, Methodology, Investigation, Formal analysis, Data curation, Conceptualization. **Volker Wulfmeyer:** Writing – review & editing, Resources, Methodology, Funding acquisition, Conceptualization. **Tsegaye Tadesse:** Writing – review & editing, Resources, Conceptualization. **Kirsten Warrach-Sagi:** Writing – review & editing, Visualization, Validation, Supervision, Methodology, Investigation, Conceptualization. **Thomas Schwitalla:** Writing – review & editing, Supervision, Conceptualization. **Tesfaye Abebe:** Writing – review & editing, Funding acquisition, Conceptualization.

Declaration of Competing Interest

The authors have no known conflicts of interest or personal relationships that could have influenced the work presented in this research. There are no financial ties that might make our research look biased. The authors declare no competing interests.

Acknowledgments

This research was funded by the German–Ethiopian SDG Graduate School: Climate Change Effects on Food Security (CLIFOOD) established by the the University of Hohenheim (Germany) and the Hawassa University (Ethiopia) and financially supported by the German Academic Exchange Service (DAAD) program "Bilateral SDG Graduate Schools" funded by the Federal Ministry for Economic Cooperation and Development (BMZ). The authors would like to thank EMI of Ethiopia, ERA5, NCEP and CHIRPS data sources for providing the data sets.

Data availability

Data will be made available on request.

References

Abara, M., Budiastuti, S., 2020. Drought frequency, severity, and duration monitoringbased on climate change in southern and southeastern Ethiopia. In: IOP Conference Series:Earth and Environmental Science, 477. IOP Publishing, 012011.

Adnan, S., Ullah, K., Gao, S., 2015. Characterization of drought and its assessment overSindh, Pakistan during 1951–2010. J. Meteorol. Res. 29 (5), 837–857.

Aghakouchak, A., 2015. A multivariate approach for persistence-based drought prediction: application to the 2010–2011 East Africa drought. J. Hydrol. 526, 127–135.

Aghakouchak, A., Feldman, D., Stewardson, M.J., Saphores, J.D., Grant, S., Sanders, B., 2014. Australia's drought: lessons for California. Science 343 (6178), 1430–1431.

Alemu, Z.A., Dioha, E.C., Dioha, M.O., 2021. Hydro-meteorological drought in Addis Ababa: A characterization study. AIMS Environ. Sci. 8 (2).

Altieri, M.A., Koohafkan, P., 2008. TWN). In: Enduring farms: climate change, smallholders and tradetional farming communities, 6. Third World Network, Penang.

Anderson, W., Cook, B.I., Slinski, K., Schwarzwald, K., McNally, A., Funk, C., 2023. Multiyear la niña events and multiseason drought in the horn of africa. J. Hydrometeorol. 24 (1), 119–131.

Bae, H., Ji, H., Lim, Y.J., Ryu, Y., Kim, M.H., Kim, B.J., 2019. Characteristics of droughtpropagation in South Korea: Relationship between meteorological, agricultural, and hydrological droughts. Nat. Hazards 99 (1), 1–16.

Bayissa, Y.A., Moges, S.A., Xuan, Y., Van Andel, S.J., Maskey, S., Solomatine, D.P., Griensven, A.V., Tadesse, T., 2015. Spatio-temporal assessment of meteorological droughtunder the influence of varying record length: the case of Upper Blue Nile Basin, Ethiopia. Hydrol. Sci. J. 60 (11), 1927–1942.

Bayissa, Y., Tadesse, T., Demisse, G., Shiferaw, A., 2017. Evaluation of satellite based rainfall estimates and application to monitor meteorological drought for the Upper Blue Nile Basin, Ethiopia. Remote Sens. 9 (7), 669.

Benson, M.A., et al., 2018. "Soil temperature response to surface climate change: The role ofthermal properties. J. Soil Sci. 54 (4), 1234–1245.

Berhanu, B., Seleshi, Y., Melesse, A.M., 2014. Surface water and groundwater resources ofEthiopia: potentials and challenges of water resources development. Nile River Basin. Ecohydrol. Chall. Clim. Change Hydropolitics 97–117.

Bogale, G.A., Erena, Z.B., 2022. Drought vulnerability and impacts of climate change onlivestock production and productivity in different agro-Ecological zones of Ethiopia. J. Appl. Anim. Res. 50 (1), 471–489.

Chai, Q., Gan, Y., Zhao, C., Xu, H.L., Waskom, R.M., Niu, Y., Siddique, K.H., 2016. Regu-lated deficit irrigation for crop production under drought stress. A review. Agron. Sustainable Dev. 36, 1–21.
Copernicus Climate Change Service (C3S)(2019): ERA5-Land hourly data from 1950 to present.Copernicus Climate Change Service (C3S) Climate Data Store (CDS). DOI:10.24381/cds.e2161bac.
Dai, A., Zhao, T., Chen, J., 2018. Climate change and drought: a precipitation and evapora-tion perspective. Curr. Clim. Change Rep. 4, 301–312.
Degefu, M.A., Bewket, W., 2015. Trends and spatial patterns of drought incidence in theomo ghibe river basin, ethiopia. Geogr. Ann. Ser. A Phys. Geogr. 97 (2), 395–414.
Devi, S., 2022. Climate change driving east Africa towards famine. Lancet 400 (10347), 150–151.
Dike, V.N., Lin, Z.H., Ibe, C.C., 2020. Intensification of summer rainfall extremes overNigeria during recent decades. Atmosphere 11, 1084. https://doi.org/10.3390/atmos11101084.
Diro, G.T., Grimes, D.I.F., Black, E., 2011. Teleconnections between Ethiopia an summerrainfall and sea surface temperature: part II. Seasonal forecasting. Clim. Dyn. 37, 121–131.
E. K. S, 2002. Drought and Famine in Ethiopia: A Study of the 2000-2001 Crisis. InternationalJournal of Environmental Studies, 59(1), 17-32.
Fan, Y., Van Den Dool, H., 2004. Climate Prediction Center global monthly soil moisture data set at 0.5 resolution for 1948 to present. J. Geophys. Res. Atmos. 109 (D10).
Fang, C., Moncrieff, J.B., 2006. The dependence of soil respiration on temperature. Soil Biol. Biochem. 38 (2), 215–225.
FAO. (2016). El Niño and Its Impact on Ethiopia. Food and Agriculture Organization of theUnited Nations.
Farahmand, A., AghaKouchak, A., 2015. A generalized framework for Derive nonparametric standardized drought indicators. Adv. Water Resour. 76, 140–145.
FEWS NET, 2021. The eastern Horn of Africa faces an exceptional prolonged and Persistent agro-pastoral drought sequence ICPAC/FEWS NET/FAO GIEWS/WFP/JRC Tech. Rep., 8 pp.,⟨https://mars.jrc.ec.europa.eu/asap/⟩ files/special_focus_2021_11.pdf.
Fuentes, I., Padarian, J., Vervoort, R.W., 2022. Spatial and temporal global patterns ofdrought propagation. Front. Environ. Sci. 10, 788248.
Funk, C., Peterson, P., Landsfeld, M., Pedreros, D., Verdin, J., Shukla, S., Husak, G., Row land, J., Harrison, L., Hoell, A., et al., 2015. The climate hazards infrared precipitation with a stationsA new environmental record for monitoring extremes. Sci. Data 2 (150066), 621.
Ge, W., Han, J., Zhang, D., Wang, F., 2021. Divergent impacts of droughts on vegetation phenology and productivity in the Yungui Plateau, southwest China. Ecol. Indic. 127, 107743.
Gebrehiwot, T., Van der Veen, A., Maathuis, B., 2011. Spatial and temporal assessment of drought in the Northern highlands of Ethiopia. Int. J. Appl. Earth Obser vation Geoinf. 13 (3), 309–321.
Gisila, T., Seid, J., Shemelis, A., Gebremariam, T., Jember, G., Amsalu, A., Mengistu, G., Mengistu, S., 2015. Ethiopian Panel on Climate Change First Assessment Report, Working Group I Physical Science Basis. Published by Ethiopian Academy of Sciences.
Gocic, M., Trajkovic, S., 2013. Analysis of changes in meteorological variables using Mann Kendall and Sen's slope estimator statistical tests in Serbia. Glob. Planet. Change 100, 172–182.
Gringorten, I.I., 1963. A plotting rule for extreme probability paper. J. Geophys Res 68 (3), 813. https://doi.org/10.1029/JZ0, 68i003p00813.
Hao, Z., AghaKouchak, A., 2013. Multivariate standardized drought index: a parametric multi-index model. Adv. Water Resour. 57, 12–18.
Hao, Z., AghaKouchak, A., 2014. A nonparametric multivariate multi-index drought monitoring framework. J. Hydrometeorol. 15 (1), 89–101.
Heydari, H., Valadan Zoej, M., Maghsoudi, Y., Dehnavi, S., 2018. An investigation of drought prediction using various remote-sensing vegetation indices for different time spans. Int. J. Remote Sens. 39 (6), 1871–1889.
Houghton, J.T., Ding, Y., Griggs, D.J., et al., 2001. Climate Change 2001: The Scientific Basis. Cambridge University Press.
Intergovernmental Panel on Climate Change (IPCC)., 2021. Sixth Assessment Report (AR6). Cambridge University Press.
Jiang, T., Su, X., Singh, V.P., Zhang, G., 2022. Spatio-temporal pattern of ecological droughts and their impacts on health of vegetation in Northwestern China. J. Environ.l Manag. 305, 114356.
Jin, M.S., Mullens, T., 2014. A study of the relations between soil moisture, soil temperatures and surface temperatures using ARM observations and offline LM4 simulations. Climate 2 (4), 279–295.
Kaniewski, D., Van Campo, E., Weiss, 2012. Drought is a recurring challenge in the Middle East. Proc. Natl. Acad. Sci. 109 (10), 3862–3867.
Karnieli, A., Agam, N., Pinker, R.T., Anderson, M., Imhoff, M.L., Gutman, G.G., Panov, N., Goldberg, A., 2010. Use of NDVI and land surface temperature for drought assessment: Merits and limitation. J. Clim. 23 (3), 618–633.
Kasie, T.A., Demissie, B.S., Bahry, M.J., Gessesse, G.M., Wale, L.E., 2020. The impact of the 2015 El Niño-induced drought on household consumption: evidence from rural Ethiopia. Clim. Dev. 12 (9), 854–863.
Kebede, A., Raju, U.J.P., Korecha, D., Nigussie, M., 2020. Developing new drought indices with and without climate signal information over the Upper Blue Nile. Model. Earth Syst. Environ. 6, 151–161.
Kendall, M.G., 1975. Rank Correlation Methods. Charles Griffin, London. Google Sch.
Kikstra, J.S., Nicholls, Z.R., Smith, C.J., Lewis, J., Lamboll, R.D., Byers, E., Sandstad, M., Meinshausen, M., Gidden, M.J., Rogelj, J., Kriegler, E., 2022. The IPCC Sixth Assessment Report WG-III climate assessment of mitigation path ways: from emissions to global temperatures. Geosci. Model Dev. 15 (24), 9075–9109.
Kleidon, A., Renner, M., 2013. A simple explanation for the sensitivity of the hydrologic cycle to surface temperature and solar radiation and its implications for global climate change. Earth Syst. Dyn. 4 (2), 455–465.
Kourouma, J.M., Eze, E., Kelem, G., Negash, E., Phiri, D., Vinya, R., Girma, A., Zenebe, A., 2022. Spatiotemporal climate variability and meteorological drought characterization in Ethiopia. Geomat. Nat. Hazards Risk 13 (1), 2049–2085.
Li, Z., Bai, X., Tan, Q., Zhao, C., Li, Y., Luo, G., Chen, F., Li, C., Ran, C., Zhang, S., Xiong, L., 2024. Dryness stress weakens the sustainability of global vegetation cooling. Sci. Total Environ. 909, 168474.
Liu, H., et al., 2020. "Effects of moisture content on soil thermal properties. Geoderma 375, 114–122.
Liu, S., Xue, L., Xiao, Y., Yang, M., Liu, Y., Han, Q., Ma, J., 2024. Dynamic process of ecosystem water use efficiency and response to drought in the Yellow River Basin, China. Sci. Total Environ. 934, 173339.
Lobell, D.B., Schlenker, W., Costa-Roberts, J., 2011. Climate trends and global crop produc tion since 1980. Science 333 (6042), 616–620.
Mahmoudi, P., Rigi, A., Miri Kamak, M., 2019. A comparative study of precipitation-based drought indices with the aim of selecting the best index for drought monitoring in Iran. Theor. Appl. Climatol. 137, 3123–3138.
Mann, H.B., 1945. Nonparametric tests against trend. Économ. J. Econom. Soc. 245–259.
Marcus, H.G., 1994. A History of Ethiopia. University of California Press.
Matere, J., Simpkin, P., Angerer, J., Olesambu, E., Ramasamy, S., Fasina, F., 2020. Predictive Livestock Early Warning System (PLEWS): Monitoring forage condition and implications for animal production in Kenya. Weather Clim. Extrem. 27, 100209.
McKee, T.B., Doesken, N.J., Kleist, J., 1993. The Relationship of Drought Frequency And Duration to Time Scales. Proc. 8th Conf. Appl. Climatol. 17, 179–183.
Mengistu, D., 2016. Impacts of drought and conventional coping strategies of Borana community, southern Ethiopia. Res. Humanit. Soc. Sci. 6 (23), 29–37.
Menna, B.Y., Mesfin, H.S., Gebrekidan, A.G., Siyum, Z.G., Tegene, M.T., 2022. Meteorological drought analysis using copula theory for the case of upper Tekeze river basin, Northern Ethiopia. Theor. Appl. Climatol. 149 (1-2), 621–638.
Mishra, A.K., Singh, V.P., 2010. A review of drought concepts. J. Hydrolgy 391 (1-2), 202–216.
Nalley, D., Adamowski, J., Khalil, B., Ozga-Zielinski, B., 2013. Trend detection in surface Air temperature in Ontario and Quebec, Canada during 1967–2006 using the discrete wavelet transform. Atmos. Res. 132, 375–398.
Omondi, O.A., Lin, Z., 2023. Trend and spatial-temporal variation of drought characteristics over equatorial East Africa during the last 120 years. Front. Earth Sci. 10, 1064940.
Palchaudhuri, M., Biswas, S., 2014. Analysis of meteorological drought using Standardized recipitation Index–A case study of Puruliya district, West Bengal, India. Int. J. Environ. Ecol. Eng. 7 (3), 167–174.

Palmer, W.C., 1965. Meteorological Drought. Research Paper No, 45. U.S. Weather Bureau.
Pankhurst, R., 1990. The History of Famine and Pestilence in Ethiopia. Addis Ababa University Press.
Philip, S., Kew, S.F., van Oldenborgh, G.J., Otto, F., O'Keefe, S., Haustein, K., King, A., Zegeye, A., Eshetu, Z., Hailemariam, K., Singh, R., 2018. Attribution analysis of the Ethiopian drought of 2015. J. Clim. 31 (6), 2465–2486.
Rulinda, C.M., Dilo, A., Bijker, W., Stein, A., 2012. Characterising and quantifying vegetative drought in East Africa using fuzzy modelling and NDVI data. J. Arid Environ. 78, 169–178.
Saddique, N., Khaliq, A., Bernhofer, C., 2020. Trends in temperature and precipitation extremes in historical (1961–1990) and projected (2061–2090) periods in a data scarce mountain basin, northern Pakistan. Stoch. Environ. Res. Risk Assess. 34, 1441–1455.
Sawada, Y., Koike, T., 2016. Towards ecohydrological drought monitoring and prediction using a land data assimilation system: A case study on the Horn of Africa drought (2010–2011). J. Geophys. Res. Atmos. 121 (14), 8229–8242.
Schlesinger, W.H., Andrews, J.A., 2000. Soil respiration and the global carbon cycle. Biogeochemistry 48 (1), 7–20.
Teshome, A., Zhang, J., 2019. Increase of extreme drought over Ethiopia under climate warming. Adv. Meteorol. 2019, 1–18.
Tesso, G., 2019. Clim. Change Nat. Disaster Rural Poverty Ethiop.
Tigkas, D., Vangelis, H., Tsakiris, G., 2017. An enhanced effective reconnaissance drought index for the characterization of agricultural drought. Environ. Process. 4, 137–148.
1984 U.S. Agency for International Development (USAID)., 1985. Ethiopia: The Great Famine of, -85. USAID Reports.
Vicente Serrano, S.M., Beguería, S., López-Moreno, J.I., 2011. Comment on "Characteristics and trends in various forms of the Palmer Drought Severity Index (PDSI) during 1900–2008" by Aiguo Dai.Wardlow, B.D., Anderson, M.C. and Verdin, J.P. eds., 2012. Remote sensing of drought: Innovative monitoring approaches. CRC Press.
Viste, E., Korecha, D. and Sorteberg, A., 2013. Recent drought and precipitation tendencies in Ethiopia. Theoretical and Applied Climatology, 112, pp.535-551.
Wagaw, M., Coleman, T., Tsegaye, T. and Tadesse, W., 2005, April. GIS implementation to support poverty reduction policy and drought management in Ethiopia. In Fourth Meeting of the Committee on Development Information (CODI IV), Addis Ababa, Ethiopia.
Wang, H., et al., 2019. Thermal dynamics in soil and the implications for ecosystem responses. Environ. Res. Lett. 14 (5), 054012.
Wardlow, B.D., Tadesse, T., Brown, J.F., Gu, Y., 2008. The vegetation drought response index (VegDRI): a new drought monitoring approach for vegetation. Natl. Integr. Drought Inf. Syst. (NIDIS) Knowl. Assess. Workshop Contrib. Satell. Remote Sens. Drought Monit. 1–33.
Ware, M.B., Mori, P., Warrach-Sagi, K., Jury, M., Schwitalla, T., Beyene, K.H., Wulfmeyer, V., 2022. Climate regionalization using objective multivariate clustering methods and characterization of climatic regions in Ethiopia. Meteorol. Z. 31, 431–453.
Weldesenbet, G.A., 2019. Analysis of rain fall variability for mekelle meteorological station, Northern Ethiopia (1960-2009). Civ. Environ. Res 11 (9), 2224–5790.
Wolde-Georgis, T., Gebru, A.A., Kinfe, Y.W., Bahiru, K.M., 2022. Ethiopia: Ethiopia: the case of the 2015–16 El Niño. El Niño ready nations and disaster risk reduction: 19 countries in perspective. Cham: Springer International Publishing, pp. 211–229.
World Food Programme (WFP)., 2001. Ethiopia Emergency Food Security Assessment. WFP Reports.
Yuan, M., Zhao, L., Lin, A., Wang, L., Li, Q., She, D., Qu, S., 2020. Impacts of preseason drought on vegetation spring phenology across the Northeast China Transect. Sci. Total Environ. 738, 140297.
Yue, S., Ouarda, T.B., Bobée, B., Legendre, P., Bruneau, P., 1999. The Gumbel mixed model for flood frequency analysis. J. Hydrol. 226 (1-2), 88–100.